Transient Simulation of AMB Supported Electric Motor during Rotor Drop on Retainer Bearings

Antti Kärkkäinen, and Aki Mikkola

Department of Mechanical Engineering
Lappeenranta University of Technology
Lappeenranta, Finland
akarkkai@lut.fi, mikkola@lut.fi

Jussi Sopanen

Faculty of Technology
South Carelia Polytechnic
Lappeenranta, Finland
jussi.sopanen@scp.fi

Abstract – **Active magnetic bearings present a new technology which has many advantages compared to traditional bearing designs. Active magnetic bearings, however, require retainer bearings in order to prevent damages in the event of a component, power or control loop failure. In the drop-down situation the design parameters of the retainer bearings have a significant influence on the behavior of the rotor. In this study, the dynamics of an active magnetic bearings supported electric motor when the rotor is dropped on retainer bearings is studied using a multibody simulation model. The retainer bearings are modeled using a detailed ball bearing model, which accounts damping and stiffness properties, oil film and friction between races and rolling elements. The model of the magnetic bearing system contains unbalances of the rotor and stiffness and damping properties of support. In this study, a computationally efficient contact model between the rotor and the retainer bearings is proposed.**

Index Terms – **Retainer bearing, Drop-down simulation, Ball bearing model, Contact model.**

I. INTRODUCTION

The area of Active Magnetic Bearings (AMBs) has recently been developed intensively because it represents a non-contact support system that has several advantages compared to conventional bearings. Due to improved materials, controller strategies, and electric components, the performance and reliability of AMBs is enhancing. Despite that, additional bearings, the so-called retainer bearings, have a vital role in the AMB applications. The most crucial moment when the retainer bearings are needed is when the rotor drops from the AMBs onto retainer bearings due to component or power failure [1, 2, 3]. Without any information and knowledge of retainer bearings, there is a great chance that an AMB-rotor system self-destructs in a drop-down situation. For this reason, the objective of this research is to shed light on the design of the retainer bearings.

Retainer bearings can be categorized into three types. Bushing type bearings are simple, and consequently, inexpensive and easy to repair if necessary. On the other hand, bushing type retainer bearings have some defects, which may restrict their use in some applications. In the bushing type retainer bearings the coefficient of friction can change during the rotor's deceleration due to wearing of the sleeve. Wearing typically increases the coefficient of friction resulting in changes in the dynamic behavior of the rotor. For this reason, bushing type retainer bearings must normally be replaced after a number of high speed drop-downs. Secondly, based on a low friction coefficient, bushing type retainer bearings are unable to dissipate the energy of the rotor without a whirling motion of the rotor. Retainer bearings of the rolling element bearing type are more complicated and, therefore, they are also more sensitive to impact. The rolling element bearing increases the power dissipation of the rotor during drop-down because the inner race rapidly achieves the angular velocity of the rotor. This may prevent the whirling motion of the rotor, as Fumagalli [4] noted. The last type of retainer bearing is a combination of the two mentioned above. This type has some beneficial features, as mentioned. However, it also has some drawbacks, such as a larger moment of inertia of rotating parts than rolling element bearing have.

The most examined characteristics of retainer bearings are the stiffness, damping and the friction coefficients between the rotor and bearing. Influences of those coefficients are widely known as pointed out by Ecker [5], Zeng [6] and Ishii and Kirk [1]. Also force calculation and knowledge of the orbit of a rotor during contact are useful despite the used bearing type, as Fumagalli [4] showed. Cole *et al*. [7] examined the dynamic behavior of a rolling element bearing following rotor impact successfully. They pointed out that the inner race of the bearing should be allowed to accelerate as rapidly as possible in order to maximize the energy dissipation of the rotor. Raju *et al*. [8] performed a similar examination as Cole *et al*. [7] using solid brass backup bearings. Both of the results are useful, but only when designing similar retainer bearings as they examined. Dynamic behavior of bushing and rolling bearing type retainer bearings can be distinguished, as the investigations of Fumagalli [4] and Swanson *et al*. [9] proved. In this topic, a number of inventive examinations have been done. For example, Wang and Noah [10] examined an accurate model of a sleeve auxiliary bearing during the rotor's drop-down. They concluded that the system should be designed to avoid operation at the speed of the free-free eigenmodes of the rotor. This should be accounted for in the drop-down situation, since it can lead to chaotic behavior. That is why a non-linear dynamical analysis is critical for the specific design of the rotor-retainer bearing system.

Common to all above-mentioned examinations is that they are based on the finite element model, rotor dynamic calculation or experimental studies. The objective of this work is to build a more accurate model of the AMB system during the rotor drop-down using a multibody simulation approach. In addition, parameters of retainer bearings are modified in order to find their contribution to the dynamic responses during the drop-down. The retainer bearings are modeled by using a detailed ball bearing model, which includes damping and stiffness properties, oil film and friction between the races and rolling elements. The model also includes combined inertias of rotating parts. The model of the AMB system includes unbalances of the rotor and stiffness and damping properties of the support.

II. DESIGN PARAMETERS OF BACKUP BEARING

A. Stiffness of Bearing and Support

Wang and Noah [10] noted that the higher the bearing stiffness, the higher the full clearance backward whirling speed and the amplitude of whirling after drop-down of the rotor. They proposed that the bearing support stiffness could be selected at a value close to the stiffness of the shaft in the auxiliary bearing design. Zeng [6] noted in his research that suitable soft support stiffness could reduce the nonlinear resonance and hence prevent the whirling motion of the rotor. One should also remember that the vibration amplitude must be small enough to ensure that the rotor does not touch other parts of the assembly.

B. Damping of Bearing and Support

Ishii and Kirk [1] noted that in the cases of very low and high support damping, a backward whirl occurs shortly after the rotor has dropped onto the backup bearings. The backward whirl may lead to a large contact force. Therefore, the optimum support-damping ratio C_{bb}/C_{sh}, where C_{bb} is the backup bearing damping and C_{sh} is the unsupported shaft damping, is between 30 and 100. In this range, the backward whirl does not occur.

Ishii and Kirk [1] also noted that for small support damping ($C_{bb}/C_{sh} \leq 5$) the maximum rotor response and the maximum contact force are sensitive to the constraint in the rotational movement of the bearing. These kinds of constraints, such as the nonlinearity of the contact point, could exist for the AMB machinery, which operates for long periods without stops.

C. Friction Coefficient between Rotor and Retainer Bearing

Ecker [5] noticed that for large values of friction coefficients, the rotor establishes a backward whirling motion. Also Fumagalli and Schwitzer [11] noted that a low coefficient of friction is a beneficial feature for the retainer bearings. It is important to note that the coefficient of friction is not always constant. This is due to wear that can occur during the interaction between the rotor and retainer bearings and, thereby, increase the value of the friction coefficient. A support with high stiffness will increase the friction coefficient rapidly and soon lead to full-clearance backward whirling motion of the rotor.

Sun [12] examined thermal growth of the retainer bearing during the contact. He noted that rotor drop dynamics and thermal growth drastically change when the friction coefficient increases from 0.25 to 0.30. Because of a larger friction force, the orbit of a rotor extends after drop-down and the first bounce direction approaches the tangential direction of the contact point. Hence, it is important to find a threshold friction coefficient above of which the rotor enters into a high-speed backward whirl. Therefore, reducing the friction coefficient is critical to the stability of the rotor drop dynamics. A fine surface finish and powder or solid lubricants can be utilized on the contact area if it is acceptable in practice.

III. MODELS OF ROTOR AND BACKUP BEARING

A. Model of the Rotor

In this paper, the rotor is modeled using a multibody simulation approach. In this approach, the motion of each body of the system is described using generalized coordinates. For body i, the vector of generalized coordinates $\mathbf{q}_r^i$ can be written as [13]

$$\mathbf{q}_r^i = \begin{bmatrix} \mathbf{R}^{iT} & \boldsymbol{\theta}^{iT} \end{bmatrix}^T , \tag{1}$$

where $\mathbf{R}^i$ is the position vector of the origin of a local coordinate system of the body and $\boldsymbol{\theta}^i$ is the vector of generalized orientation coordinates. The orientation of the body can be described using, for example, Euler angles, Rodriguez parameters or Euler parameters. By using generalized coordinates, the global position of an arbitrary particle P on body i can be expressed in the following form:

$$\mathbf{r}^i = \mathbf{R}^i + \mathbf{A}^i \overline{\mathbf{u}}^i , \tag{2}$$

where $\mathbf{A}^i$ is a rotation matrix that describes the rotation of the local coordinate system with respect to the global coordinate system and $\overline{\mathbf{u}}^i$ is the position vector of a particle in the local coordinate system. The velocity of an arbitrary particle can be obtained by differentiating (2) with respect to time as follows:

$$\dot{\mathbf{r}}^i = \dot{\mathbf{R}}^i + \dot{\mathbf{A}}^i \overline{\mathbf{u}}^i , \tag{3}$$

where $\dot{\mathbf{A}}^i \overline{\mathbf{u}}^i$ can be written as

$$\dot{\mathbf{A}}^i \overline{\mathbf{u}}^i = -\mathbf{A}^i \tilde{\overline{\mathbf{u}}}^i \overline{\mathbf{G}}^i \dot{\boldsymbol{\theta}}^i , \tag{4}$$

where $\tilde{\overline{\mathbf{u}}}^i$ is the skew symmetric matrix of vector $\overline{\mathbf{u}}^i$. Matrix $\overline{\mathbf{G}}^i$ defines the relationship between the angular velocities in the local body frame and the time derivatives of the orientation coordinates as follows:

$$\overline{\boldsymbol{\omega}}^i = \overline{\mathbf{G}}^i \dot{\boldsymbol{\theta}}^i . \tag{5}$$

It is important to point out that the expressions of the rotation matrix $\mathbf{A}^i$ and matrix $\overline{\mathbf{G}}^i$ depend on the selected generalized orientation coordinates. By using Lagrange's equation and an augmented formulation for the kinematic constraints, the system equation of motion can be written as follows [14]

$$\mathbf{M}\ddot{\mathbf{q}} + \mathbf{C_q}^T\boldsymbol{\lambda} = \mathbf{Q}_e + \mathbf{Q}_v , \qquad (6)$$

where $\mathbf{M}$ is the mass matrix, $\mathbf{C_q}$ the constraint Jacobian matrix, $\boldsymbol{\lambda}$ the vector of Lagrange multipliers, $\mathbf{Q}_e$ the vector of generalized forces and $\mathbf{Q}_v$ the vector of the quadratic velocity inertia forces, which contains the terms that are quadratic in the velocities, such as the gyroscopic and Coriolis terms. The mass matrix of body i can be obtained from the expression of the kinetic energy as follows:

$$T^i = \frac{1}{2}\int_{V^i} \rho^i \dot{\mathbf{r}}^{iT}\dot{\mathbf{r}}^i dV^i = \frac{1}{2}\dot{\mathbf{q}}_r^{iT}\mathbf{M}^i\dot{\mathbf{q}}_r^i , \qquad (7)$$

where V^i is the volume of body i and $\mathbf{M}^i$ the mass matrix.

The externally applied forces must be defined as generalized forces that affect the system's generalized coordinates. Using the principle of the virtual work, the generalized forces caused by globally applied forces $\mathbf{F}^i$ and moments $\mathbf{T}^i$ can be expressed as [13]

$$\left(\mathbf{Q}_e^i\right)_R = \mathbf{A}^i\mathbf{F}^i \qquad (8)$$

$$\left(\mathbf{Q}_e^i\right)_\theta = \left(\mathbf{A}^i\overline{\mathbf{G}}^i\right)^T\left(\mathbf{A}^i\widetilde{\overline{\mathbf{u}}}_P^i\mathbf{A}^i\mathbf{F}^i + \mathbf{A}^i\mathbf{T}^i\right) , \qquad (9)$$

where $\left(\mathbf{Q}_e^i\right)_R$ and $\left(\mathbf{Q}_e^i\right)_\theta$ are the vectors of the generalized forces associated with the translational and rotational generalized coordinates of body i, respectively. Vector $\overline{\mathbf{u}}_P^i$ defines the working point of the force in the local coordinate system.

The kinematical constraint equations are functions of the system's generalized coordinates and can be expressed as follows:

$$\mathbf{C}\left(\mathbf{q}_r, t\right) = \mathbf{0} . \qquad (10)$$

The constraint Jacobian matrix can be obtained by differentiating the constraint equations with respect to the generalized coordinates as follows:

$$\mathbf{C_q} = \frac{\partial \mathbf{C}\left(\mathbf{q}_r, t\right)}{\partial \mathbf{q}_r} . \qquad (11)$$

Equation (6) represents the dynamic equations of the constrained system. For numerical integration it can be re-arranged as follows

$$\begin{bmatrix} \mathbf{M} & \mathbf{C_q}^T \\ \mathbf{C_q} & \mathbf{0} \end{bmatrix}\begin{bmatrix} \ddot{\mathbf{q}}_r \\ \boldsymbol{\lambda} \end{bmatrix} = \begin{bmatrix} \mathbf{Q}_e + \mathbf{Q}_v \\ \mathbf{Q}_c \end{bmatrix} , \qquad (12)$$

where

$$\mathbf{Q}_c = -\mathbf{C}_{tt} - \left(\mathbf{C_q}\dot{\mathbf{q}}_r\right)_{\mathbf{q}}\dot{\mathbf{q}}_r - 2\mathbf{C}_{\mathbf{q}t}\dot{\mathbf{q}}_r . \qquad (13)$$

The acceleration vector and the vector of Lagrange multipliers $\boldsymbol{\lambda}$ can then be solved from (12).

B. Model of the Ball Bearing

Sopanen and Mikkola [15, 16] presented and implemented a six degree-of-freedom dynamic model of a deep-groove ball bearing. The model of the bearing included descriptions of non-linear Hertzian contact deformation and elastohydrodynamic fluid film thickness. The geometry, such as the outer and inner diameter of the bearing and clearances, and material properties are given as an input to the model. The bearing force and torque components are calculated from the relative displacements and velocities between bearing rings. The torque around the rotation axis of the bearing is caused by friction and consists of three components: viscous friction torque, load-dependent friction torque and seal friction.

C. Model of the Contact

Usually commercial multibody programs, such as MSC.ADAMS, include built-in contact models [17]. That kind of contact is usually created to be generalized and multipurpose, and therefore, the calculation of contact may require a significant computational capacity. Thus it is important to create a contact model that works effectively and foreseeably every moment during the simulation. In addition, in this way it is possible to create a friction model without insignificant parameters. Contact between the rotor and the bearing is modeled using a circle-in-circle contact, which is presented in Fig. 1.
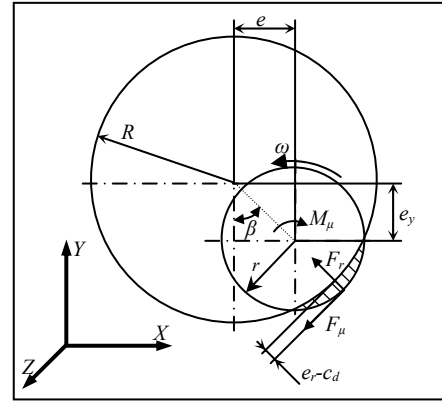
Fig. 1 Circle-in-circle contact.

The radial contact force F_r is a function of the contact penetration and the penetration velocity. The radial contact force, which affects the rotor, can be written as follows

$$F_r = \max\begin{cases} \begin{cases} K(e_r - c_d)^e + f(e_r, c_d, 0, d, C)\cdot\dot{e}_r \; ; \; e_r \geq c_d \\ 0 \qquad\qquad\qquad ; \; e_r < c_d \end{cases} \\ 0 \end{cases} , (14)$$

where K is stiffness of the contact and C is damping of the contact. The exponent e is the force-deflection relationship. The X- and Y-components of the radial

contact force F_r can be calculated using the geometry presented in Fig. 1. Radial displacement e_r and velocity $\dot{e}_r$ between the rotor and the sleeve can be obtained from the displacements along the X- and Y-axes as follows

$$e_r = \sqrt{e_x^2 + e_y^2} \tag{15}$$

$$\dot{e}_r = \frac{e_x \dot{e}_x + e_y \dot{e}_y}{\sqrt{e_x^2 + e_y^2}} . \tag{16}$$

Clearance in the contact c_d can be obtained from radiuses of the rotor r and the sleeve R as follows

$$c_d = R - r . \tag{17}$$

To avoid discontinuities in the contact force, the velocity-dependent terms are smoothed using cubic polynomial expression, which is defined by (18). Thus, at zero penetration, the damping coefficient C is zero. The parameter d in (14) is the radial displacement when a maximum damping coefficient is achieved. The polynomial expression can be defined as

$$f(g, g_0, h_0, g_1, h_1) = \begin{cases} h_0 & ; \ g \leq g_0 \\ h_0 + \Delta h \cdot \Delta g^2 (3 - 2\Delta g) & ; \ g_0 < g < g_1 \\ h_1 & ; \ g \geq g_1 \end{cases}, \tag{18}$$

where $\Delta h = h_1 - h_0$ and $\Delta g = (g - g_0)/(g_1 - g_0)$. Variable g is an independent variable, while g_0 and g_1 are the starting and ending values of the step. Correspondingly, h_0 and h_1 are the initial and final values.

The magnitude of the friction force, which acts on the center of the rotor and is perpendicular to the radial contact force, can be calculated as follows

$$F_\mu = \frac{\omega_{diff}}{|\omega_{diff}|} \cdot \mu \cdot F_r \cdot f(\omega_{diff}, 0, 0, \omega_l, 1), \tag{19}$$

where μ is the coefficient of friction between the rotor and bearings. Parameter ω_{diff} describes the difference of angular velocities between the rotor and the sleeves and can be written as $\omega_{diff} = \omega_r - \omega_s$, where ω_r and ω_s are the angular velocities of the rotor and the sleeves. The parameter ω_l describes the threshold angular speed above which the friction coefficient μ achieves the maximum value. The friction force causes a friction torque M_μ, the direction of which is opposite to the direction of rotation.

IV. STUDIED STRUCTURE

The studied structure is an electrical motor, whose rotor is supported by two AMBs. The structure includes also retainer bearings (6016 type, deep-groove ball bearing), which have a vital role in the case of emergency drop-down. The test rotor can be seen in Fig. 2. Both AMB forces, F_{AMB1} and F_{AMB2}, will shut down immediately when a fault situation occurs, which means that the collapsing magnetic field will not generate any forces at all. On the inner rings of the retainer bearings (RB$_1$ and RB$_2$ in Fig. 2)

are sleeves that are rigidly connected to the inner rings of the bearings. The air gap between the sleeves and the rotor is half of the air gap of the AMBs. The outer rings of the retainer bearings are rigidly mounted on the bearing housings. For simplicity, the bearing housings have only two degrees of freedom, namely translations in the global X- and Y-directions. The housings are connected to the ground with linear spring-dampers in the above-mentioned directions. The stiffness coefficients are the same in both directions, as well as the damping coefficients. The dimensions of the motor are shown in Table I and properties of the used retainer bearings are shown in Table II. The direction of gravity g is the negative Y-direction. The unbalance mass UB is located in the middle of the rotor at an angle of 90º from the positive X-axis and at a distance of 97.5 mm from the rotation axis. The parameters of the contacts between the rotor and the sleeves are shown in Table III.
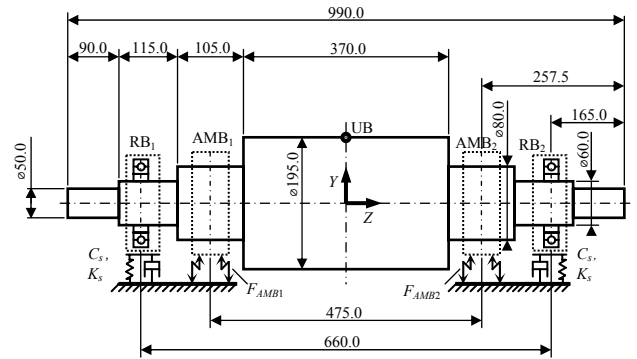
Fig. 2 Diagram of the electric motor under investigation. Dimensions are in millimeters.

TABLE I
PARAMETERS OF THE STUDIED ELECTRIC MOTOR

Mass of the rotor, m	97.3 kg
Polar moment of inertia of the rotor, I_p	0.39 kgm^2
Diametral moments of inertia of the rotor, I_d	2.82 kgm^2
Air gap between rotor and sleeves	300 μm
Inner diameter of sleeve, d_{si}	60.6 mm
Outer diameter of sleeve, d_{so}	80.0 mm
Gravity constant, g	9.80665 m/s^2

TABLE II
PARAMETERS OF THE TYPE 6016 RETAINER BEARING

Bore diameter, d_B	80.0 mm
Outer diameter, D_O	125.0 mm
Bearing width, B	22.0 mm
Pitch diameter, d_m	110.0 mm
Ball diameter, d_b	19.05 mm
Number of balls, z	10
Diametral clearance, c_d	15 μm
Bearing damping coefficient, c_b	0.25 Ns/mm
Inner and outer race conformity, R_r	0.52
Static load rating, C_0	40 000 N
Modulus of elasticity, E	206 000 MPa
Poisson's ratio, ν	0.3
Viscosity parameter, α	0.023 mm^2/N
Viscosity parameter, η_0	0.04·10^{-6} Ns/mm^2

TABLE III
PARAMETERS OF THE CONTACT

Stiffness coefficient of the contact, K	$1\cdot10^8$ N/m
Damping coefficient of the contact, C	1000 Ns/m
The contact parameter, d	0.01 mm
Exponent of the force-deflection relationship, e	1.1
Threshold angular speed, ω_l	10 rpm

V. SIMULATION RESULTS

In this section, the effects of the friction coefficient and the stiffness and damping coefficients of the support on responses and contact forces are examined. The total time of the simulation is 1 second and AMBs are turned off when the simulation has proceeded 0.1 seconds. The initial angular velocity of the rotor is 10000 rpm.

A. Effect of Friction Coefficient

In this section the responses, the orbit of the rotor, the contact forces of the support, and the velocities of the sleeve are studied with different friction coefficients μ. The unbalance mass m_{UB} is 1 g, the stiffness of the support K_s is $5\cdot10^7$ N/m and the damping of the support C_s is 5000 Ns/m. Fig. 3 shows the orbits of the rotor at the retainer bearing 1 when the friction coefficient is varied. The rotor starts to whirl when the friction coefficient between the rotor and the sleeves is 0.39. Fig. 3 shows that the orbit of the rotor becomes larger as the friction coefficient increases. This can be seen even before the rotor starts to whirl. In the whirling motion, the orbit of the rotor increases significantly. The largest motion does not occur immediately after the drop-down, as in the case of lower friction coefficients. The largest responses occur after 0.08 seconds of the drop-down. After this moment, the responses, i.e. the orbit of the rotor, are stabilized. The orbit of the rotor does not stay inside of the static retainer bearing, the circle in Fig. 3, after the drop-down. This is due to the fact that the retainer bearings are assembled elastically on the ground and the bearing model describes the compression of the bearing, as well.

The coefficient of friction has a vital role for contact forces if the rotor experiences a violent backward whirl, as can be seen in Fig. 4. If the rotor stays at the bottom of the sleeves, the contact forces are approximately the same during the deceleration in all cases. However, when the rotor started to whirl the contact forces increased significantly; the forces are two times larger than in the case where the rotor stays at the bottom of the sleeves. This should be accounted for in mechanical design.

Angular velocities of the sleeves depend on two parameters: the friction coefficient and the skid between the sleeves and the rotor. If the discrepancy between the rotation velocities of the rotor and the sleeves is large, the sleeve accelerates more rapidly than if its rotation velocity is near the rotation velocity of the rotor. When the rotor starts to whirl, the sleeves accelerate much faster than in the case when the rotor stays at the bottom of the sleeves. The reason for this kind of behavior is the constant contact between the rotor and sleeves. Immediately after the drop-down, the rotor bounces back and forth as can be noted in

Fig. 3. This behavior causes steps to the curve describing the angular velocities of the sleeves. This can be seen especially in the situation where the rotor starts to whirl. In the simulation, it is assumed that the friction coefficient between the rotor and the sleeves is the same throughout the simulation. This may be unreal, because the friction coefficient changes depending on the rotor's and sleeves' temperatures and wearing.
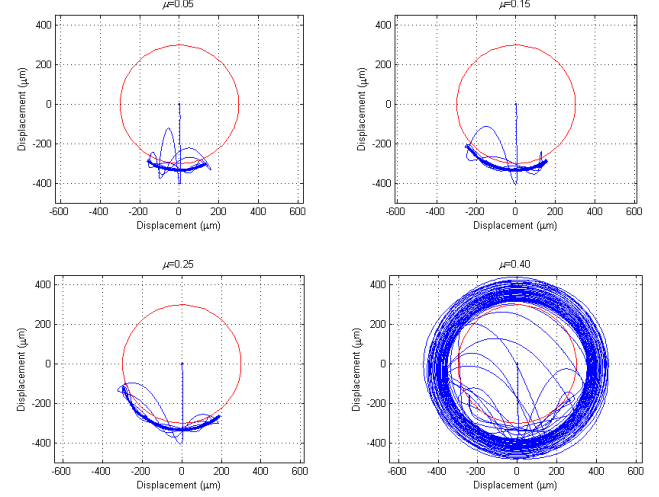
Fig. 3 Orbits of the rotor.
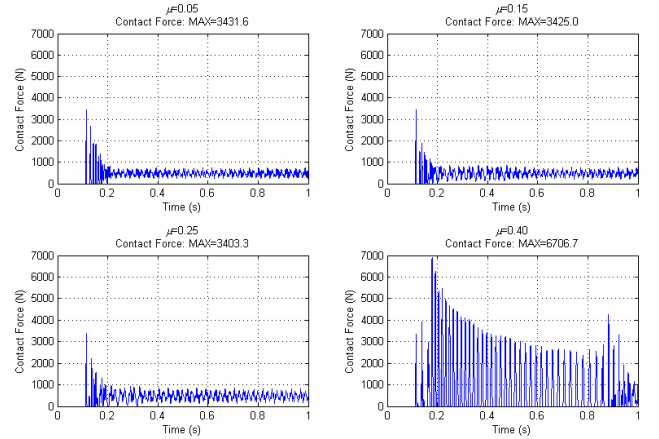
Fig. 4 Contact forces of the support.

B. Effect of Stiffness and Damping Coefficients of Support

The examination that presents the rotor's responses with the stiffness coefficient of the support $K_s=5\cdot10^6$ N/m and $K_s=5\cdot10^8$ N/m shows clearly that the stiffness of the support has a vital role when defining the response. Because the responses are directly dependent on the support's stiffness and the contact forces on the responses, the stiffness of the support determinates the behavior of the rotor after the drop-down. This is the case especially when the friction coefficient is smaller than the threshold friction, as in this case ($\mu=0.25$, $C_s=5000$ Ns/m). The largest response of the rotor in the Y-direction with $K_s=5\cdot10^6$ N/m comes immediately after the drop-down of the rotor and its value is near to 600 μm. This is absolutely the maximum acceptable value of the responses, because the air gaps of the AMBs were 600 μm. In this case, the

responses stabilized quickly unlike in the case of a harder supported rotor. This occurred despite the fact that the value of relative damping is the same in both cases. The comparison of the orbits between the harder supported and softer supported cases shows that displacements of the stiffer case are minimal compared to the softer case. This leads to the problem that the contact forces in the case of K_s=5·10^8 N/m are two times larger than in the case presented in the section above and almost five times larger than in the softer supported case in this section.

The large damping coefficient of the support leads to a more stable chaotic response of the rotor after the drop-down. In the more damped case, C_s=27900 Ns/m, the orbit of the rotor is smoother than in the low damped case, C_s=2790 Ns/m. This means that vibrations and noises are also smaller in the more damped case than in the low damped case. Correspondingly, the contact forces stabilize faster in the more damped case than in the low damped case. Based on the above-mentioned, the importance of the damping coefficient with stiffness coefficient is significant.

VI. CONCLUSIONS

In this study, the dynamics of the AMB system during rotor drop-down in the failure incident was investigated using the multibody simulation approach. The studied structure includes the rotor, two AMBs and two retainer ball bearings which included sleeves on the inner rings. Using this model, the effects of retainer bearing parameters on system vibration were examined. The examination of the AMB system implies that the multibody simulation approach is an efficient procedure for the rotor-retainer bearing simulation. Particularly, the bearing model and the contact models in the multibody approach are efficient and suitable for drop-down simulation.

The results of this paper are in good agreement with studies available in the literature. The AMB system under investigation needs a high friction coefficient between the rotor and sleeves before full backward whirling motion of the rotor occurs. This is in agreement with the previous examination of AMBs [18]. However, it is possible that in practical experiments the rotor can experience whirling motion with lower threshold friction than in the simulations. This is due to the inaccuracies in the friction model. From a practical point of view, the inaccurate friction model is due to the use of a constant friction coefficient which did not account for the increase of the friction coefficient resulting from thermal growing and wearing in sleeves [19]. The stiffness coefficient and the damping coefficient of the support play a vital role in the behavior of the rotor during and after the rotor's drop-down. Particularly, the contact forces between the rotor and the retainer bearings are dependent on the stiffness of the support.

This research introduces important information for the design of retainer bearings of the physical prototype. The most important results were the critical values for the friction, stiffness and damping coefficients. The simulation results also shed a light on the magnitude of the contact forces during the drop-down of the rotor. Multibody

simulation proved to be an effective tool when studying the contact dynamics between the rotor and the retainer bearings. The prototype of the studied structure is currently under examination and the results of this research will be verified experimentally in the near future.

REFERENCES

[1] Ishii, T., and Kirk, R. G., 1996, "Transient Response Technique Applied to Active Magnetic Bearing Machinery During Rotor Drop," *ASME Journal of Vibration and Acoustics*, **118**, pp. 154-163.

[2] Schweitzer, G., Bleuler, H., and Traxler, A., 1994, *Active Magnetic Bearings - Basics, Properties and Applications*, vdf Hochschulverlag AG, Zurich.

[3] Orth, M., Erb, R., and Nordmann, R., 2000, "Investigations of the Behavior of a Magnetically Suspended Rotor during Contact with Retainer Bearings," *Proceedings of 7th ISMB*, Zurich, Switzerland, August, ETH Zurich, pp. 33-38.

[4] Fumagalli, M. A., 1997, Modelling and Measurement Analysis of the Contact Interaction between a High Speed Rotor and its Stator, Doctoral Dissertation, Swiss Institute of Technology, Zurich.

[5] Ecker, H., 1998, "Nonlinear Stability Analysis of a Single Mass Rotor Contacting a Rigid Backup Bearing," *Dynamics of Vibro-Impact Systems: Proceedings of the Euromech Colloquium: 15-18 September 1998*, Loughborough, United Kingdom, September, Springer Verlag, pp. 79-89.

[6] Zeng, S., 2002, "Motion of AMB Rotor in Backup Bearings," *ASME Journal of Vibration and Acoustics*, **124**, pp. 460-464.

[7] Cole, M. O. T., Keogh, P. S., and Burrows, C. R., 2002, "The Dynamic Behavior of a Rolling Element Auxiliary Bearing Following Rotor Impact," *ASME Journal of Tribology*, **124**, pp. 406-413.

[8] Raju, K. V. S., Ramesh, K., Swanson, E. E., and Kirk, R. G., 1995, "Simulation of AMB Turbomachinery for Transient Loading Conditions," *Proceedings of MAG'95*, Alexandria, USA, August, Technomics Publishers Co., pp. 227-235.

[9] Swanson, E. E., Kirk, R. G., and Wang, J., 1995, "AMB Rotor Drop Initial Transient on Ball and Solid Bearings," *Proceedings of MAG'95*, Alexandria, USA, August, Technomics Publishers Co., pp. 207-216.

[10] Wang, X., and Noah, S., 1998, "Nonlinear Dynamics of a Magnetically Supported Rotor on Safety Auxiliary Bearings," *ASME Journal of Vibration and Acoustics*, **120**, pp. 596-606.

[11] Fumagalli, M., and Schweitzer, G., 1996, "Motion of Rotor in Rigid Retainer Bearings," *Proceedings of 5th International Symposium on Magnetic Bearings*, Kanazawa, Japan, August, pp. 509-514.

[12] Sun, G., 2006, "Rotor Drop and Following Thermal Growth Simulation Using Detailed Auxiliary Bearing and Damper Models," *Journal of Sound and Vibration*, **289**, pp. 334-359.

[13] Shabana, A. A., 2001, *Computational Dynamics, 2nd Edition*, John Wiley & Sons, New York.

[14] Shabana, A. A., 1998, *Dynamics of Multibody Systems, 2nd Edition*, John Wiley & Sons, New York.

[15] Sopanen, J., and Mikkola, A., 2003, "Dynamic Model of a Deep Groove Ball Bearing Including Localized and Distributed Defects, Part 1: Theory", *Proceedings of the Institution of Mechanical Engineers, Journal of Multi-Body Dynamics*, **217**(K), pp. 201-211.

[16] Sopanen, J. and Mikkola, A., 2003, "Dynamic Model of a Deep Groove Ball Bearing Including Localized and Distributed Defects, Part 2: Implementation and Results", *Proceedings of the Institution of Mechanical Engineers, Journal of Multi-Body Dynamics*, **217**(K), pp. 213-223.

[17] ADAMS Online Documentation, 2001, version 12.0, Mechanical Dynamics, Inc, Ann Arbor, Michigan, USA.

[18] Foiles, W. C., and Allaire, P. E., 1997, "Nonlinear Transient Modeling of Active Magnetic Bearing Rotors during Rotor Drop on Auxiliary Bearing," *Proceedings of MAG'97*, Alexandria, USA, August, Technomics Publishers Co., pp. 154-163

[19] Zeng, S., 2003, "Modelling and Experimental Study of the Transient Response of an Active Magnetic Bearing Rotor during Rotor Drop on Back-Up Bearings," *Proceedings of the Institution of Mechanical Engineers. Part I, Journal of systems & control engineering*, **217**, pp. 505-517.